Available online at www.easdprocedia.org
EASD Procedia EURODYN (2020) 1475-1490

EASD Procedia

EURODYN 2020
XI International Conference on Structural Dynamics
M. Papadrakakis, M. Fragiadakis, C. Papadimitriou (eds.)
Athens, Greece, 23–26 November 2020

A LOCAL ACTIVE NOISE CONTROL SYSTEM BASED ON A NONLINEAR SENSING TECHNIQUE FOR YACHT APPLICATIONS

Mylonas D., Erspamer A., Paradisiotis A., Yiakopoulos C., Antoniadis I.

National Technical University of Athens, School of Mechanical Engineering, Department of Mechanical Design & Automatic Control, Laboratory of Dynamics and Structures

chryiako@cental.ntua.gr

Keywords: Nonlinear active noise control (NANC), Functional link networks (FLNs), Narrowband noise, Maritime environment.

Abstract. *Active noise control (ANC) is an important subject that plays a central role in many practical problems. In essence, the ANC technique is based on the principle that a noise can be cancelled by another noise with the same amplitude but an opposite phase. Compared with the passive noise control technique, the ANC method is efficient to suppress noise with lower frequency. As an adaptive controller, the filtered-x least mean square (FxLMS) algorithm has gained substantial popularity owing to its simplicity. Unfortunately, in the physical world, many ANC systems exhibit certain degrees of nonlinearity in the primary or secondary path. In such situations, nonlinear ANC (NANC) algorithm is necessary for further implementation. A novel nonlinear filter, which incorporates the concept of exponential sinusoidal models into nonlinear filters based on functional link networks (FLNs) has been applied in this paper. The proposed filter is designed to provide improved convergence characteristics over traditional FLN filters. The conventional trigonometric FLN (TFLN) may be considered as a special case of the proposed adaptive exponential FLN (AEFLN). An adaptive exponential least mean square (AELMS) algorithm has been derived and the same has been successfully applied for identification of a couple of nonlinear plants. This paper investigates the application of active noise control to the attenuation of the noise produced by two asynchronous generators in a luxury yacht, with the specific aim of creating a quiet region in a twin cabin around the sleeping area.*

1 INTRODUCTION

Passive noise control treatments are an effective means of reducing the levels of noise and vibration experienced by humans in a variety of applications. However, due to both weight and size restrictions their performance in practice is generally limited to the control of higher frequency noise and vibration. To overcome this limitation and achieve significant levels of low frequency noise attenuation, active control methods have been widely investigated. Ac-

ISSN:2311-9020
Peer-review under responsibility of the Organizing Committee of EURODYN 2020.
doi: 10.47964/1120.9119.19996

tive control systems reduce the unwanted primary disturbance by the introduction of secondary sources, which produce either additional noise or vibration to control the original source.

Active control has been successfully demonstrated in a variety of engineering applications where the perception of the acoustic environment is particularly important. For example, in the aircraft environment the low frequency tonal noise induced by the propellers has been successfully controlled using a feedforward active noise control system [1]. In the automotive environment a variety of active control systems have been proposed for both engine [2] and road noise control [3]. More broadly, active control technology has been applied to fan noise [4], active earmuffs [5], noise transmission through windows [6], sound radiation from a helicopter transmission [7] and diesel generator noise in the master cabin of a luxury yacht [8].

Active noise control (ANC) system is an electro-acoustic device based on the principle of destructive interference by generating the signal which has the same amplitude and opposite phase with the undesired noise. Because of the potential industrial applications and digital signal processing advantages, many different kinds of ANC algorithms are developed quickly in recent years [9, 10]. More widely used of them is filtered-x least mean square (FXLMS) algorithm based on linear finite impulse response (FIR) filter [11], which works well in most cases. However, these superiorities are only applied in linear control problem. In other words, when the reference signal measured by the acoustic sensor or the transfer functions of the primary path and secondary path are nonlinear, the ANC system based on FXLMS algorithm performs poorly and even fails to work [12].

In order to solve the nonlinear distortions in ANC system, a variety of nonlinear structures and algorithms are proposed over past fifteen years [13, 14].

Nonlinear filters based on functional link networks (FLNs) have received significant attention owing to its single layer structure, which offers lesser computational complexity and due to the simple learning rule [15]. FLN-based nonlinear system identification by using FLN-based filters has been attempted in [16] and FLN filters have found applications in other areas of nonlinear filtering including channel equalization [17] and echo cancellation [18]. In a traditional trigonometric FLN (TFLN), the input signal is functionally expanded using a set of trigonometric functions, before applying to an adaptive weight matrix. FLNs which employ other functional expansions than trigonometric functions have also been proposed recently. A Chebyshev FLN was presented in [19] for identification of dynamic systems. A Legendre neural network (LeNN), which employs a Legendre functional expansion, has been successfully applied for nonlinear channel equalization in wireless communication systems [20]. The lower computational load offered by TFLN-based nonlinear filters has made TFLN a popular candidate for nonlinear controllers in an ANC scenario also.

Thus, in this work, a nonlinear filter, which is based on an exponentially decaying trigonometric functional expansion has been applied in a yacht environment [21]. The performance of the filter has been enhanced by incorporating an adaptive exponential factor [21]. The effectiveness of the proposed filter has been tested using an extensive real world study. In this work, the filter has been shown to provide an improved noise cancellation in an ANC scenario.

2 DIESEL GENERATOR NOISE CONTROL

The acoustic environment in luxury yachts has become an important consideration for yacht manufacturers. High levels of noise and vibration can result in an uncomfortable environment and, therefore, there is a desire to achieve low levels of noise and vibration. At mid to high frequencies passive noise and vibration control treatments can be employed to achieve a quiet living space on-board. At low frequencies, however, the size and weight of passive treatments becomes too large and is often either impractical or significantly increases the

weight of the yacht, which in turn limits its efficiency. Thus, the occupants are sensitive to the noise produced by the electrical generators whilst moored.

Therefore, focus has been made on controlling the noise produced by the generators in a twin cabin, and especially when the generators are asynchronous.

Fig. 1 shows the yacht and the twin cabin considered in this work. The yacht specification are presented in the Table 1. In order to characterise the noise produced by the asynchronous generators, the sound pressure level has been measured at the head of the bed in the twin cabin using a microphone B&K model 4189 when the diesel generators are running on the mooring. The spectrum of the A-weighted sound pressure level measured by the microphone has been calculated. From the results illustrated in Figs. 6 and 7 it can be seen that the noise signal and its spectrum are characterised by an interference pattern between two sounds of slightly different frequencies, which comprise a series of harmonics of the fundamental engines orders at the mains frequencies of f_o=52 and f_1=55 Hz due to the asynchronous disturbance.

(a) (b)

Figure 1: The ANC has been applied to (a) a luxury yacht and (b) in a twin cabin.

Length (FT)	70
Beam (FT)	24
Draft (FT)	7.3
Engines	MAN 1300 X2
Generators	2X ONAN 21 KW-17 KW
Fuel (LTRS/HR)	400
Cruising Speed (KNOT/HR)	23

Table 1: Yacht specifications.

3 TFLN AND AEFLN BASED NONLINEAR FILTERS

In an FLN, the functionally expanded input signal is multiplied with a set of adaptive weights and then added together to obtain the output signal. Assuming *x(n)* as the input signal, in a TFLN, the functionally expanded signal vector may be written as:

$$f(n) = \{1, x(n), sin[\pi x(n)], \dots, sin[B\pi x(n)], cos[B\pi x(n)], x(n-1), sin[\pi x(n-1)], cos[\pi x(n-1)], \dots, x(n-N+1), sin[\pi x(n-N+1)], cos[\pi x(n-N+1)], \dots, sin[B\pi x(n-N+1)], cos[B\pi x(n-N+1)]\}^T \quad (1)$$

where B is the order of the functional expansion. The output of the TFLN may be written as:

$$y(n) = wf_o(n) + wf_1(n)x(n) + wf_2(n)sin[\pi x(n)] + wf_3(n)cos[\pi x(n)] + \cdots wf_{(M-2)}(n)sin[B\pi x(n)] + wf_{(M-1)}(n)cos[B\pi x(n)] \quad (2)$$

with $\boldsymbol{w}_f(n)=[\, w_{f0}(n), w_{f1}(n), \ldots, w_{f(M-1)}(n)]^T$ as the adaptive weight vector of the TFLN. The weights of the TFLN are usually updated using a gradient descent approach as

$$\boldsymbol{wf}(n+1) = \boldsymbol{wf}(n) + \mu te(n)\boldsymbol{f}(n) \quad (3)$$

where $e(n)$ is the error signal and μ_t is the learning rate.

It may be noted that TFLN attempts to model the nonlinearities in a system using sinusoids. Many of the natural signal-like speech which has fast amplitude variations cannot be effectively modeled using nonlinear filters based on pure sinusoids [22]. It has also been reported that the modeling of such signals can be achieved with better accuracy using sinusoids with exponentially varying amplitudes [23]. In order to overcome this limitation of pure sinusoids-based nonlinear filter like TFLN, we attempt to design a new nonlinear filter, which incorporates exponentially varying sinusoids in the modeling process. The new filter, which is hereafter referred to as AEFLN, is also designed to handle both growing as well as decaying exponential nonlinearities.

Similar to that in a TFLN, in an AEFLN, the tap delayed input signal

$$\boldsymbol{x}(n) = [x(n), x(n-1), \ldots, x(n-N+1)]T \quad (4)$$

of length N is functionally expanded to $M=N(2B+1)+1$ terms. The expanded input signal vector is given by

$$\begin{aligned}\boldsymbol{g}(n) &= \{1, x(n), e^{-\alpha(n)|x(n)|}\sin[\pi x(n)], e^{-\alpha(n)|x(n)|}\cos[\pi x(n)], \ldots, e^{-\alpha(n)|x(n)|}\sin[B\pi x(n)], \\ &e^{-\alpha(n)|x(n)|}cos[B\pi x(n)], x(n-1), e^{-\alpha(n)|x(n-1)|}\sin[\pi x(n-1)], e^{-\alpha(n)|x(n-1)|}\cos[\pi x(n-1)], \ldots, \\ &e^{-\alpha(n)|x(n-1)|}\sin[B\pi x(n-1)], e^{-\alpha(n)|x(n-1)|}\cos[B\pi x(n-1)], \ldots, x(n-N+1), e^{-\alpha(n)|x(n-N+1)|}\sin[\pi x(n-N+1)], \\ &e^{-\alpha(n)|x(n-N+1)|}\cos[\pi x(n-N+1)], \ldots, e^{-\alpha(n)|x(n-N+1)|}\sin[B\pi x(n-N+1)], \\ &e^{-\alpha(n)|x(n-N+1)|}\cos[B\pi x(n-N+1)]\}\end{aligned} \quad (5)$$

where $a(n)$ is an adaptive exponential parameter. The expanded input signal vector $\boldsymbol{g}(n)$ is multiplied by the adaptive weight vector

$$\boldsymbol{w}(n) = [wo(n), w1(n-1), \ldots, wM-1(n)]T \quad (6)$$

to obtain the filter output, which is given by

$$y(n) = w_o(n) + w_1(n)x(n) + w_2(n)sin|\pi x(n)|/\, e^{\alpha(n)|x(n)|} + w_3(n)cos|\pi x(n)|/\, e^{\alpha(n)|x(n)|} + \cdots w_{(M-2)}(n)sin|B\pi x(n)|/\, e^{\alpha(n)|x(n)|} + w_{(M-1)}(n)cos|B\pi x(n)|/\, e^{\alpha(n)|x(n)|} \tag{7}$$

(7) may be written in a compact form as

$$y(n) = \boldsymbol{g}T(n)\boldsymbol{w}(n) \tag{8}$$

The weight vector is updated as

$$\boldsymbol{w}(n+1) = \boldsymbol{w}(n) + \mu we(n)\boldsymbol{g}(n) \tag{9}$$

where μ_w is the step size. In a similar fashion, the adaptive exponential factor *a(n)* is updated as:

$$a(n+1) = a(n) + \mu\alpha e(n)\boldsymbol{z}T(n)\boldsymbol{w}(n) \tag{10}$$

where μ_a is the learning rate of *a(n)* and *z(n)* is an $M\times 1$ vector

$$\boldsymbol{z}(n) = \{0, 0, -|x(n)|\, e^{-\alpha(n)|x(n)|}\sin[\pi x(n)], -|x(n)|\, e^{-\alpha(n)|x(n)|}\cos[\pi x(n)], \ldots, -|x(n)|e^{-\alpha(n)|x(n)|}sin[B\pi x(n)], -|x(n)|e^{-\alpha(n)|x(n)|}cos[B\pi x(n)], \ldots, 0, -|x(n-N+1)|\, e^{-\alpha(n)|x(n-N+1)|}sin[\pi x(n-N+1)], -|x(n-N+1)|\, e^{-\alpha(n)|x(n-N+1)|}cos[\pi x(n-N+1)], -|x(n-N+1)|\, e^{-\alpha(n)|x(n-N+1)|}sin[B\pi x(n-N+1)], -|x(n-N+1)|\, e^{-\alpha(n)|x(n-N+1)|}cos[B\pi x(n-N+1)]\}^T \tag{11}$$

(9) and (10) together forms the adaptive exponential least mean square (AELMS) algorithm. Fig. 2 shows the block diagram of AEFLN updated using an AELMS algorithm.

4 PERFORMANCE ASSESSMENT

The effectiveness of the proposed nonlinear filter has been evaluated through an experimental study a twin cabin of a yacht (Fig. 1). The performance of AEFLN has been compared with that obtained using TFLN.

The mean square error (MSE) has been used as the metric of comparison

$$MSE = 10loog10\{E[e2(n)]\} \tag{12}$$

$$e(n) = d(n) - y(n) \tag{13}$$

where *d(n)* is the output of the system and *y(n)* is the anti-noise signal (Fig. 2).

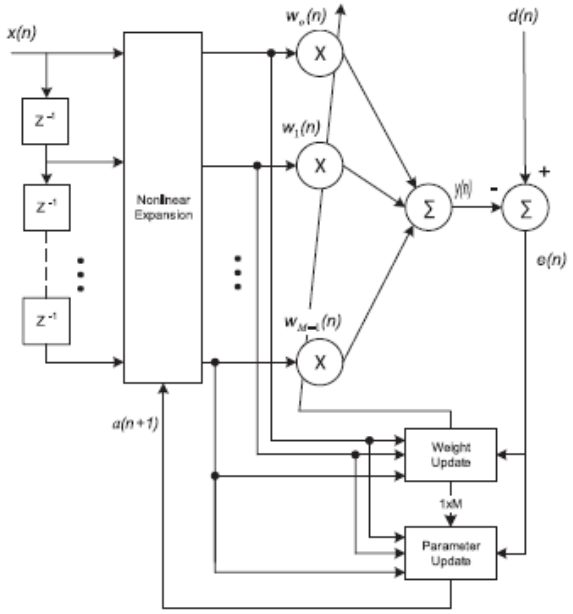

Figure 2: Block diagram of an AEFLN updated using an AELMS algorithm [21].

Initially, an attempt has been made to study the effect of the buffer size *BS* on the performance and the convergence behavior of the AEFLN-based model.

Fig. 3, shows the variations of MSE with respect to the iterations for fixed values of order *ORD*=2, learning rates μ_w=0.01 and μ_a=0.05, and initial value of a=10. As illustrated in Fig. 3, the MSEs computed over the last 3000 iterations are about -36, -28 and -18 dBs for *BS* 30, 20 and 10, respectively. Thus, the AEFLN-based ANC system has been shown to provide a better performance for buffer size greater than 30. The enhanced noise cancellation performance of AEFLN controller with respect to *BS* is confirmed in the Figs. 4 and 5. The error signal *e(n)* measured at the point of interest is presented in Fig. 6, while its spectrum is shown in Fig. 5. From those plots it can been seen that significant levels of narrowband attenuation achieved around the 'beat' components and their harmonics for *BS* greater than 30 samples. In addition to the noise attenuation performance shown in the waveforms of the Fig. 4, it is also interesting to observe the enhanced convergence behavior of the AEFLN controller.

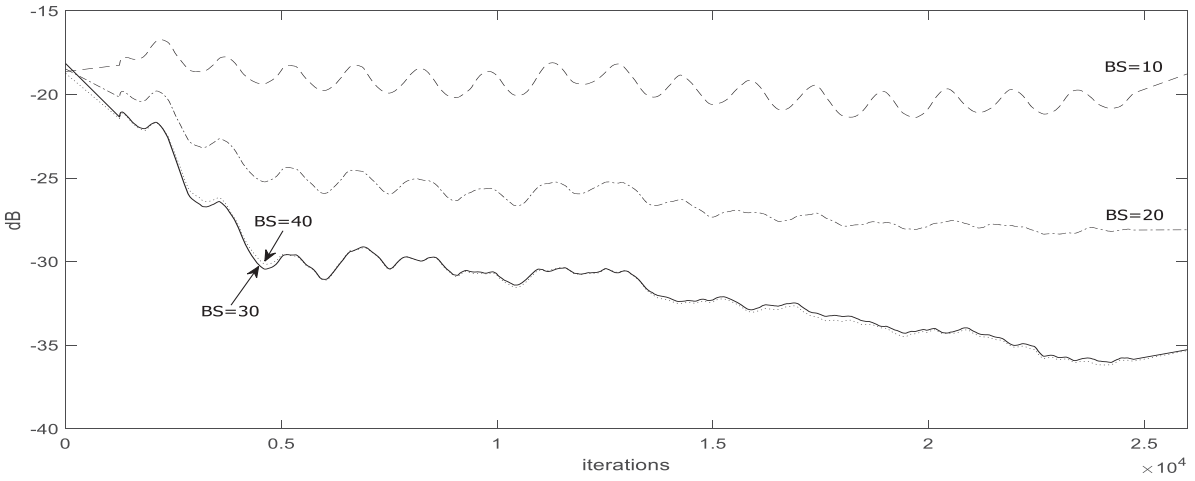

Figure 3: Comparison of convergence characteristics (MSE) obtained for different buffer sizes *BS* and AEFLN order *ORD*=2, a=10, μ_w=0.01 and μ_a=0.05.

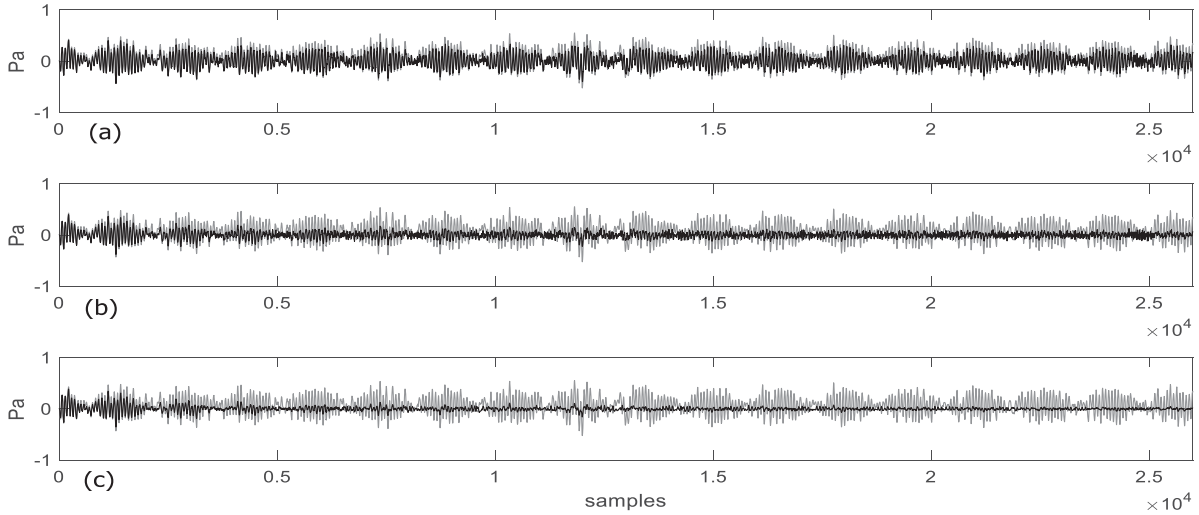

Figure 4: Error (black) and desired (gray) signals for buffer size *BS* (a) 10, (b) 20 and (c) 30 (*ORD*=2, *a*=10, μ_w=0.01 and μ_a=0.05).

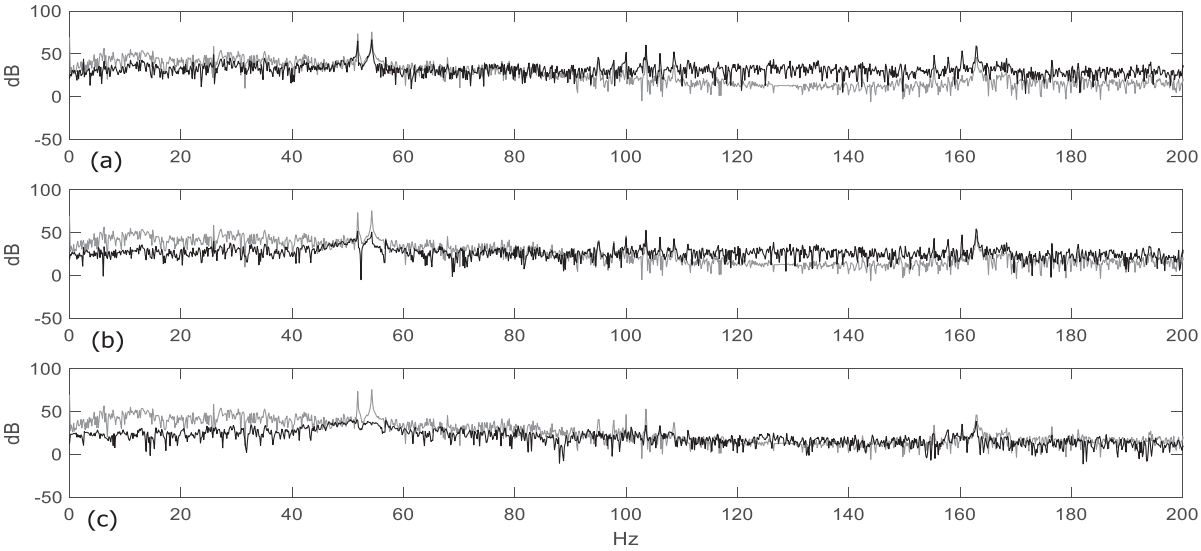

Figure 5: Spectrum of the error (black) and desired (gray) signals for buffer size *BS* (a) 10, (b) 20 and (c) 30 (*ORD*=2, *a*=10, μ_w=0.01 and μ_a=0.05).

Moreover, it may be noted, as shown in Table 2, that the ANCS using *BS*=30 achieved up to 40 dB noise reduction at the desired 'beat' components f_o and f_1.

Freq. (Hz)	ANC OFF SPL (dB)	ANC ON/SPL (dB)		
		BS=10	*BS*=20	*BS*=30
f_o=52	73.33	64.98	51.77	39.32
f_1=55	75.48	66.32	50.74	34.26

Table 2: AEFLN controller performance in accordance to the buffer size *BS*.

Then, the effect of the step size μ_w on the performance and the convergence behavior of the AEFLN controller is studied with respect to the iterations for fixed values of order *ORD*=2, buffer size *BS*=30 and μ_a=0.05, and initial condition of *a*=10.

Thus, as it is observed in Fig. 6, the MSEs computed over the last 6000 iterations are about -50, -35 and -23 dBs for μ_w 0.01, 0.001 and 0.0001, respectively. This means that the AEFLN approach achieves an improved steady state MSE for μ_w close to 0.01. Thus, the AEFLN-based ANC system has been shown to provide a better performance for step size μ_w greater than 0.01 and smaller than 0.1. Also, the noise cancellation performance of AEFLN controller with respect to step size μ_w is confirmed in the Figs. 7 and 8, and the Table 3.

The measured error signal *e(n)* and its spectrum are shown in Figs. 7 and 8. Again, a high narrowband attenuation and an enhanced convergence behavior of the AEFLN controller is achieved around the 'beat' components and their harmonics for step size μ_w close to 0.01. As shown in Table 3, that the ANCS using μ_w =0.01 achieved up to 37 dB noise reduction at the desired 'beat' components f_o and f_1.

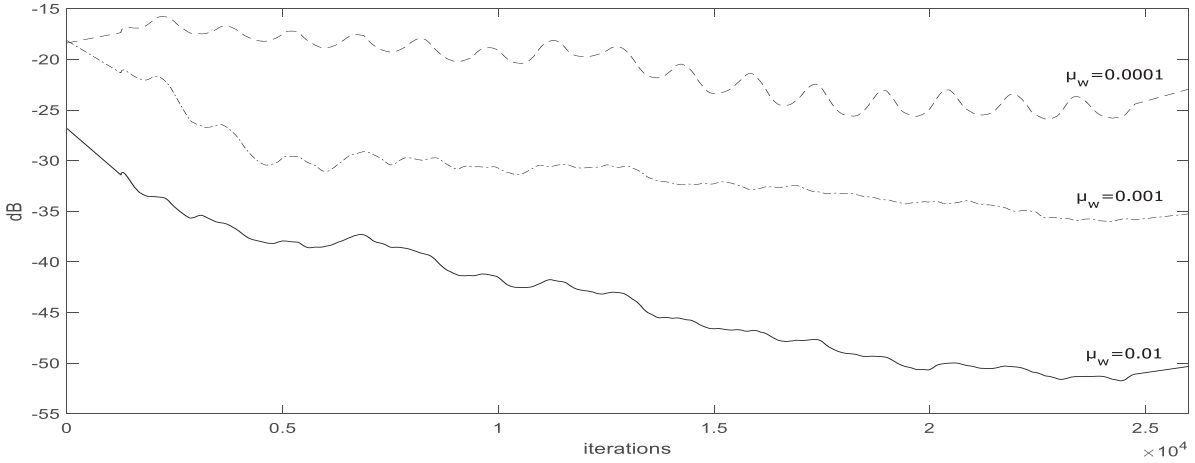

Figure 6: Comparison of convergence characteristics (MSE) obtained for different step sizes μ_w (*ORD*=2, *BS*=30, *a*=10 and μ_a=0.05.

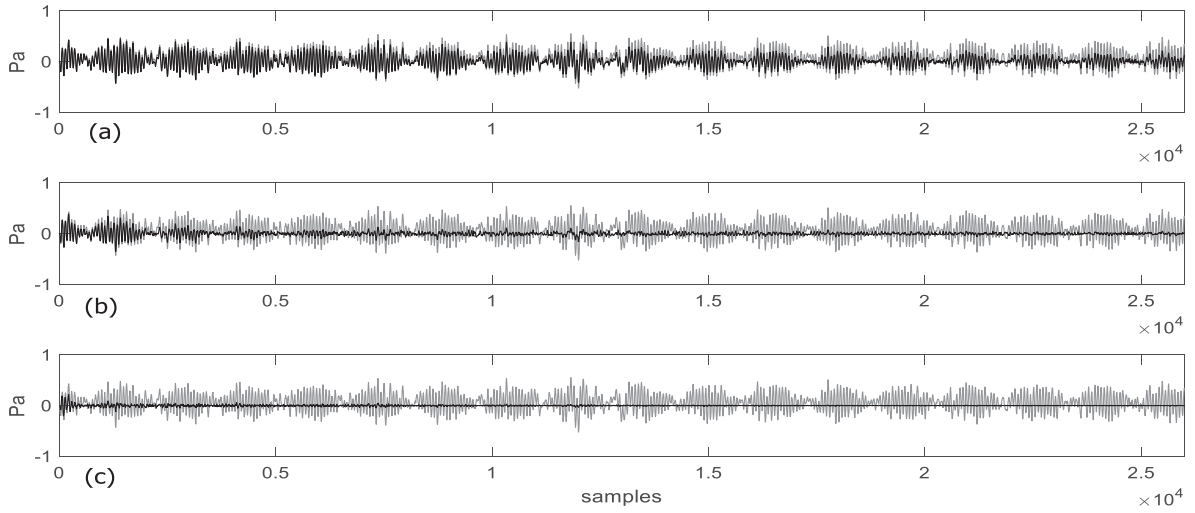

Figure 7: Error (black) and desired (gray) signals for step size μ_w (a) 0.0001, (b) 0.001 and (c) 0.01 (*ORD*=2, *BS*=30, *a*=10, μ_a=0.05).

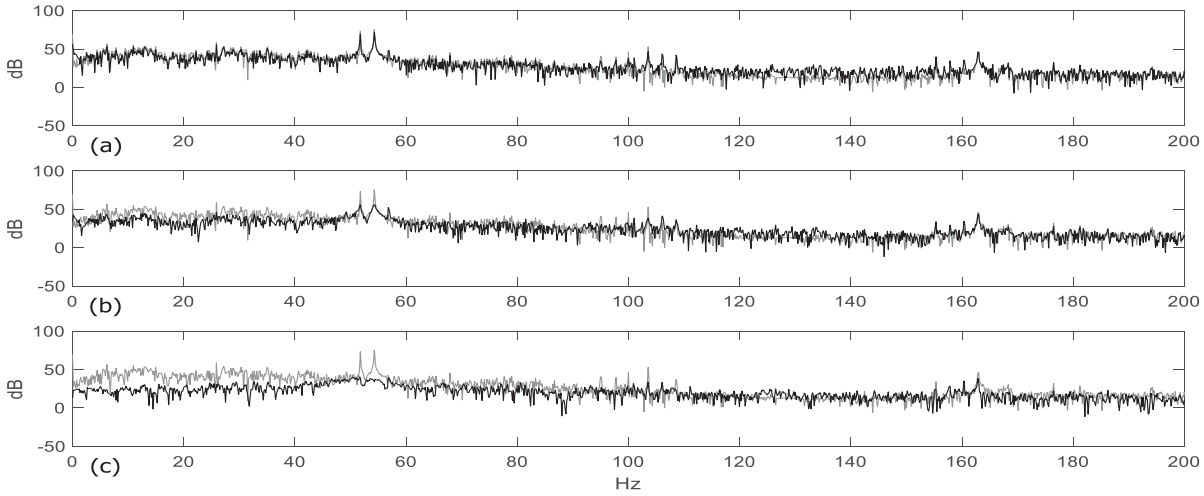

Figure 8: Spectrum of error (black) and desired (gray) signals for step size μ_w (a) 0.0001, (b) 0.001 and (c) 0.01 (*ORD*=2, *BS*=30, a=10, μ_a=0.05).

Freq. (Hz)	ANC OFF SPL (dB)	ANC ON/SPL (dB)		
		μ_w=0.0001	μ_w=0.001	μ_w=0.01
f_o=52	73.33	69.38	55.94	39.32
f_1=55	75.48	71.41	56.02	34.26

Table 3: AEFLN controller performance in accordance to the step size μ_w.

In addition, as presented in Fig. 9, the step size μ_w affects the steady state and the convergence of the exponential factor a. The attempt to study the convergence behavior of a has been achieved considering fixed values of order *ORD*=2, buffer size *BS*=30 and μ_a=0.05, and initial condition of a=10. Thus, a fast and steady convergence speed and behavior of a can be expected increasing the value of μ_w close to 0.01.

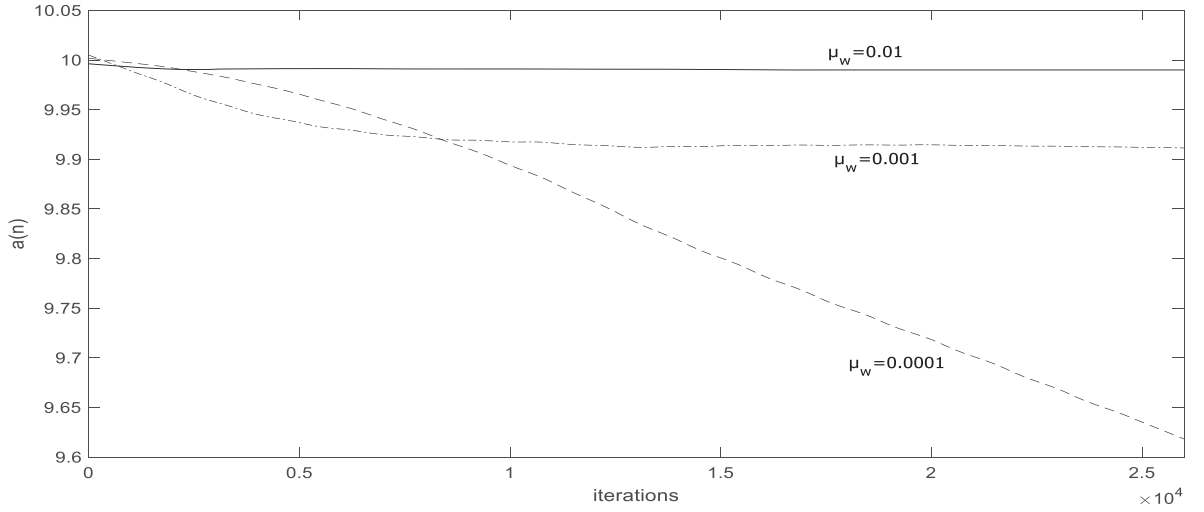

Figure 9: Exponential factor a(n) convergence for different step sizes μ_w (*ORD*=2, *BS*=30, a=10, μ_a=0.05).

Moreover, a study of the AEFLN convergence behavior in respect of the initial condition of a has been achieved considering fixed values of order ORD=2, buffer size BS=30, μ_w=0.01 and μ_a=0.05.

As it is observed in Fig. 10, the MSEs computed over the last 3000 iterations are about -60, -52, -45, -50 and -55 dBs for a equal to -1, 0, 2, 10 and 20, respectively. Thus, the convergence speed and AEFLN performance are slightly affected by the initial condition of a.

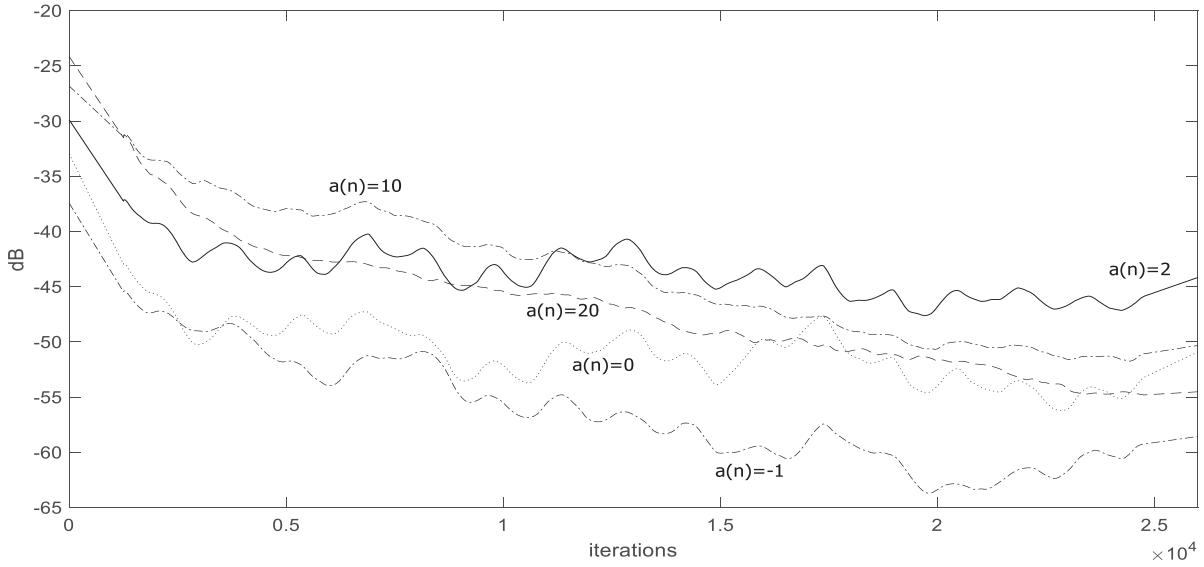

Figure 10: Comparison of convergence characteristics (MSE) obtained for different adaptive exponential parameters $a(n)$ (ORD=2, BS=30, μ_w=0.01 and μ_a=0.05).

In contrast to the buffer size and the step size μ_w, the order of the AEFLN controller in this case does not affect the convergence speed and performance of AEFLN and exponential factor a. The following results illustrated in Figs. 11 and 12 confirm the above conclusion.

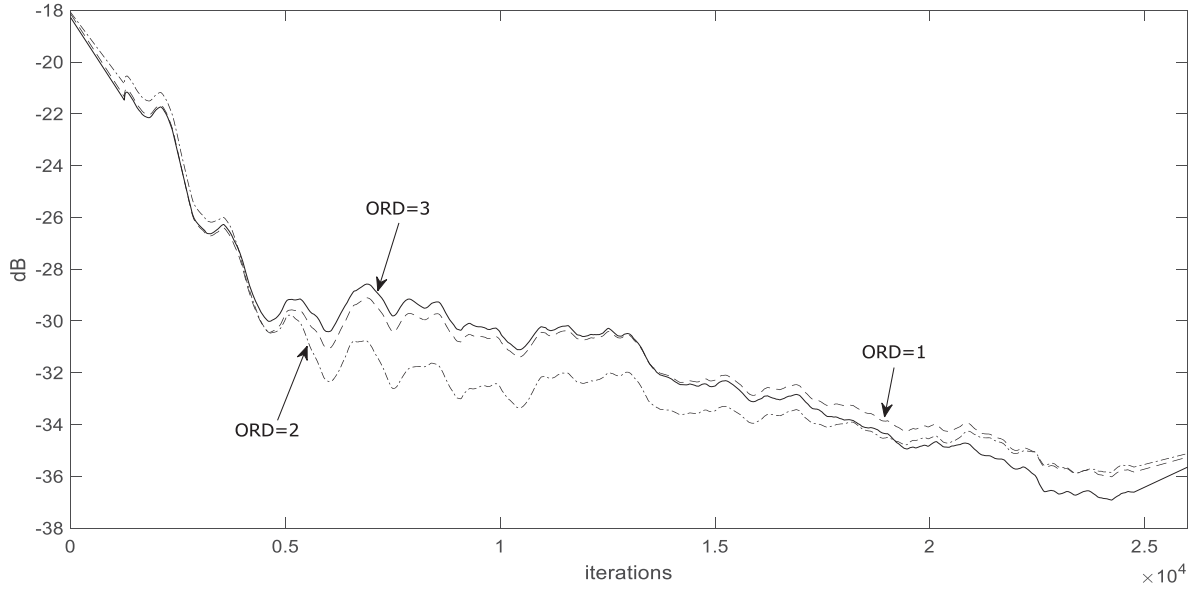

Figure 11: Comparison of convergence characteristics (MSE) obtained for different AEFLN orders (a=10, μ_w=0.01 and μ_a=0.05).

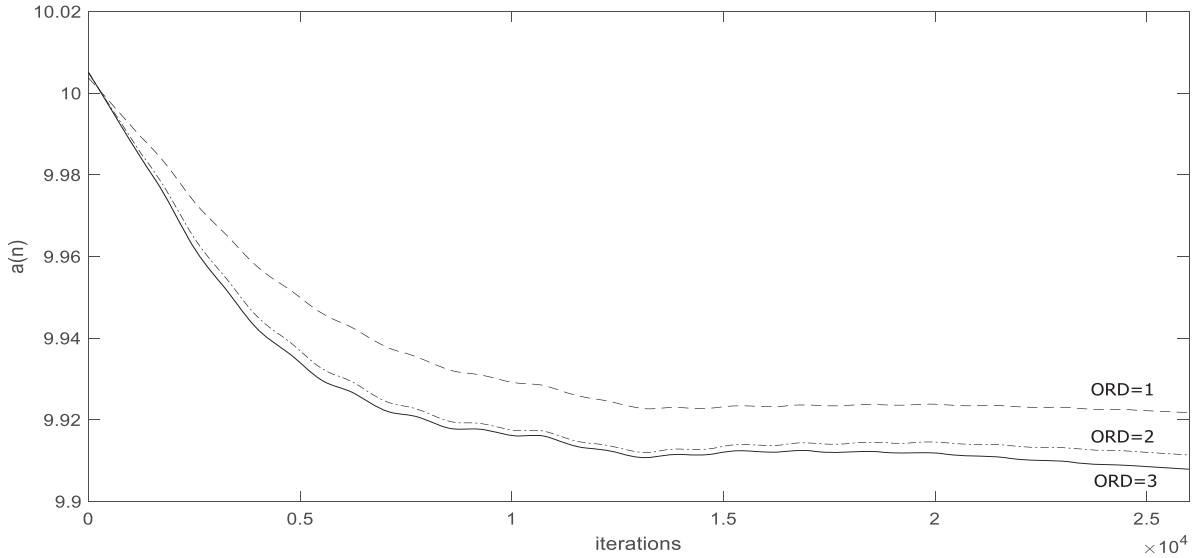

Figure 12: Exponential factor a(n) convergence for different AEFLN orders *ORD* (a=10, μ_w=0.01 and μ_a=0.05).

Next, another attempt has been made to study the effect of the buffer size *BS* on the performance and the convergence behavior of the TFLN-based controller.

Fig. 13, shows the variations of MSE with respect to the iterations for fixed values of order *ORD*=2 and learning rate μ_t=0.001. As illustrated in Fig. 13, the MSEs computed over the last 12000 iterations are about -45, -34, -23 and -20 dBs for *BS* 30, 20, 10 and 5, respectively. It is obvious that the TFLN controller provides a better performance for buffer size close to 30. Also, the Figs. 14 and 15 confirm the enhanced noise cancellation performance of TFLN controller with respect to *BS*. Figs. 14 and 15 present the error signal *e(n)* and its spectrum, respectively. The plots of Figs. 14 and 15 confirm that significant levels of narrowband attenuation achieved around the 'beat' components and their harmonics for *BS* greater than 30 samples. In the Fig. 14, it is also interesting to observe the enhanced convergence behavior of the TFLN controller.

Moreover, as shown in Table 4, the ANC system using *BS*=30 can achieve up to 45 dB noise reduction at the desired 'beat' components f_o and f_1.

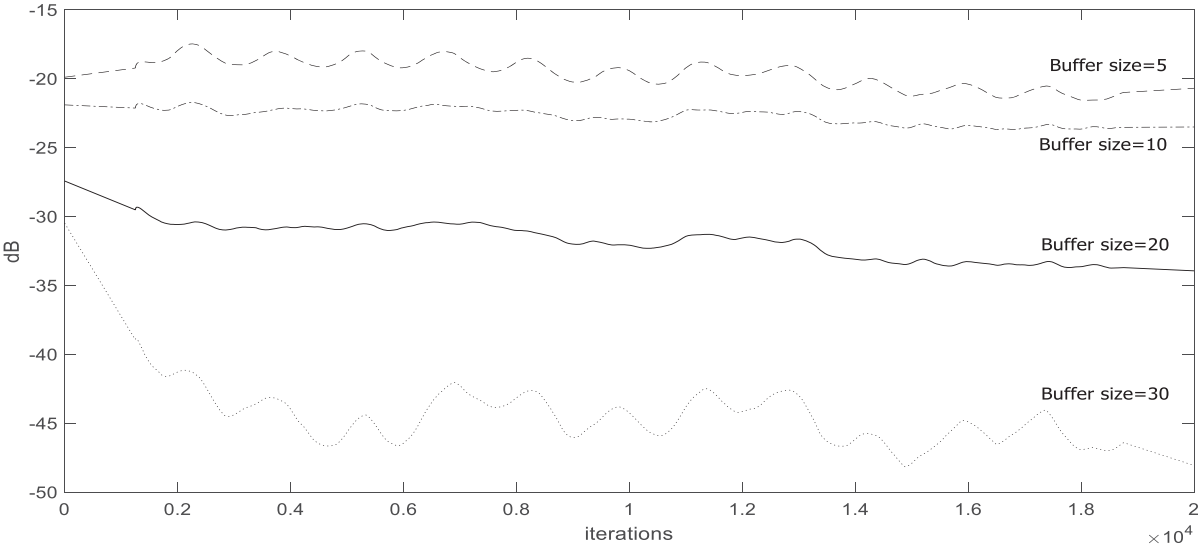

Figure 13: Comparison of convergence characteristics (MSE) obtained for different buffer sizes *BS* and TFLN order *ORD*=2, and μ_t=0.001.

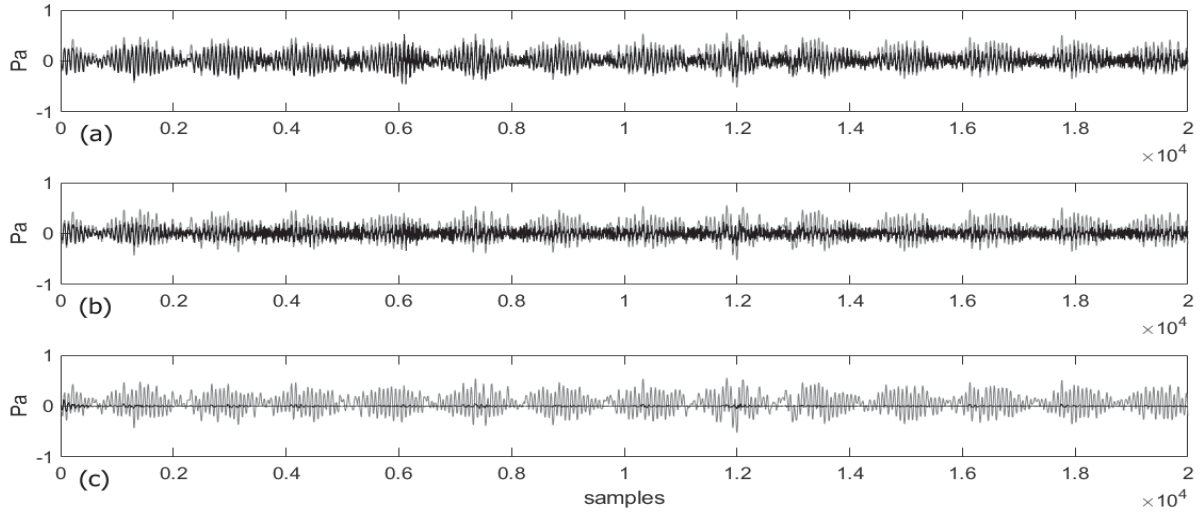

Figure 14: Error (black) and desired (gray) signals for buffer size *BS* (a) 5, (b) 10 and (c) 30 (*ORD*=2 and μ_t=0.001).

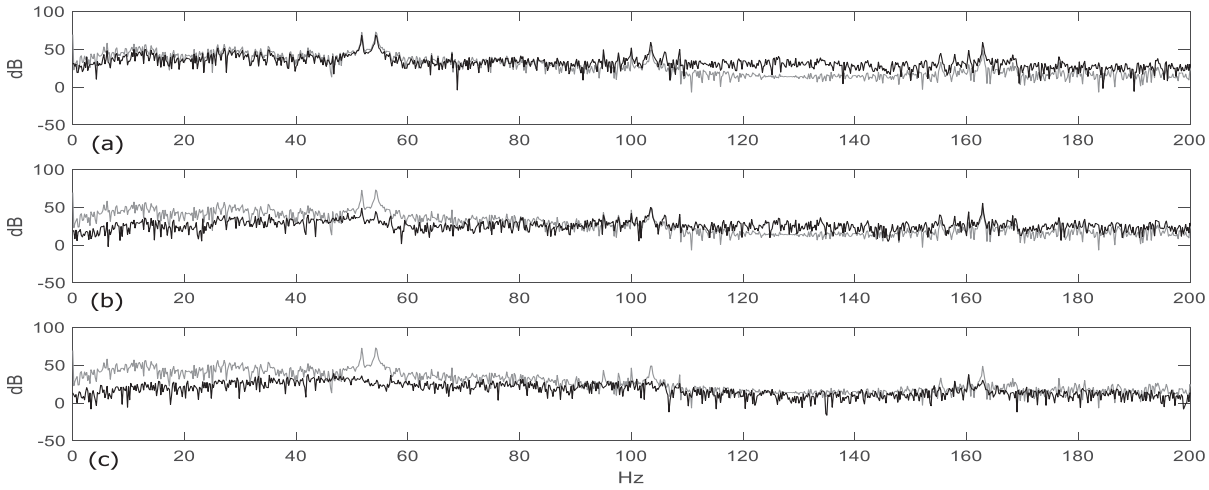

Figure 15: Spectrums of error (black) and desired (gray) signals for TFLN buffer size *BS* (a) 5, (b) 20 and (c) 30 (*ORD*=2 and μ_t=0.001).

Freq. (Hz)	ANC OFF SPL (dB)	ANC ON/SPL (dB)		
		BS=5	*BS*=20	*BS*=30
f_o=52	73.33	68.41	48.81	35.98
f_1=55	75.48	68.92	44.31	25.93

Table 4: TFLN controller performance in accordance to the buffer size *BS*.

Similarly to the AEFLN controller, the order of the TFLN controller does not affect the convergence speed and performance. The following results illustrated in Figs. 11 and 12 confirm the above conclusion.

Fig. 16, shows the variations of MSE with respect to the iterations for fixed values of buffer size *BS*=2 and learning rate μ_t=0.001. As illustrated in Fig. 16, the TFLN controller performance has slight variations in accordance to the order. Also, the Figs. 17 and 18, and the Table 5 confirm the performance and convergence speed of TFLN controller with respect to *ORD*.

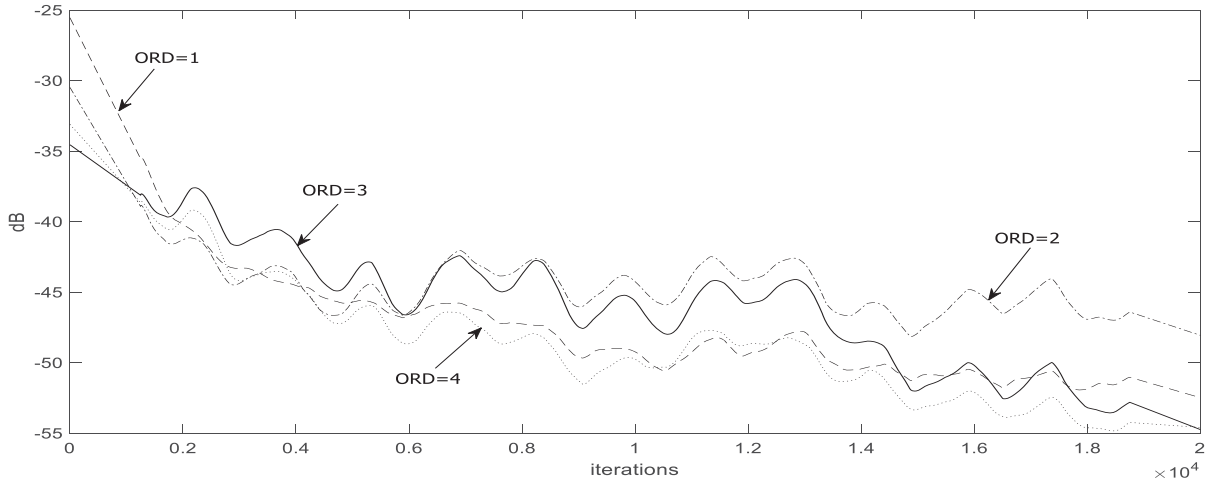

Figure 16: Comparison of convergence characteristics (MSE) obtained for different TFLN orders (μ_t=0.001 and buffer size *BS*=30).

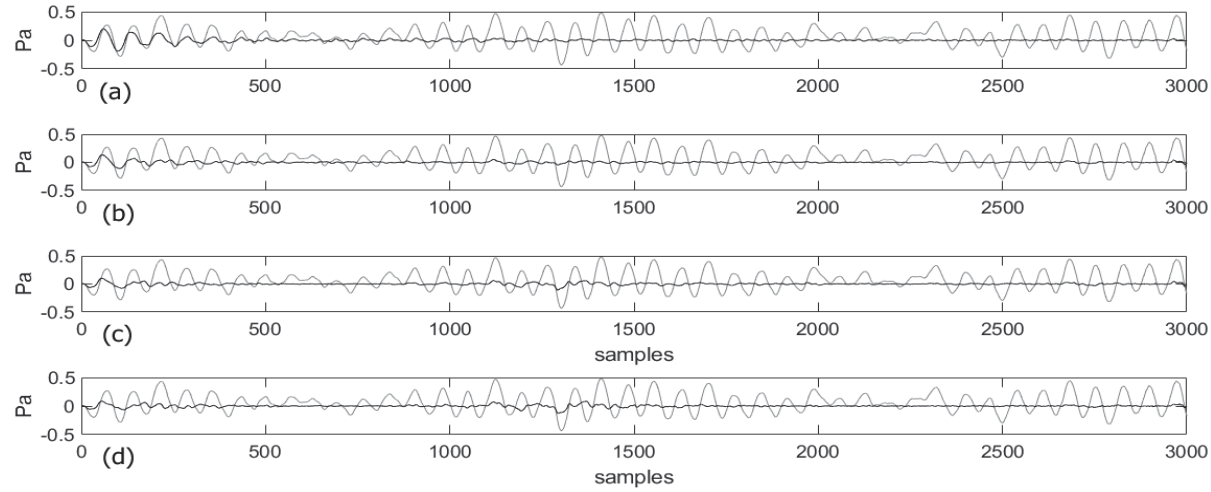

Figure 17: Error (black) and desired (gray) signals for TFLN order size (a) 1, (b) 2, (c) 3 and (d) 4 (μ_t=0.001 and *BS*=30).

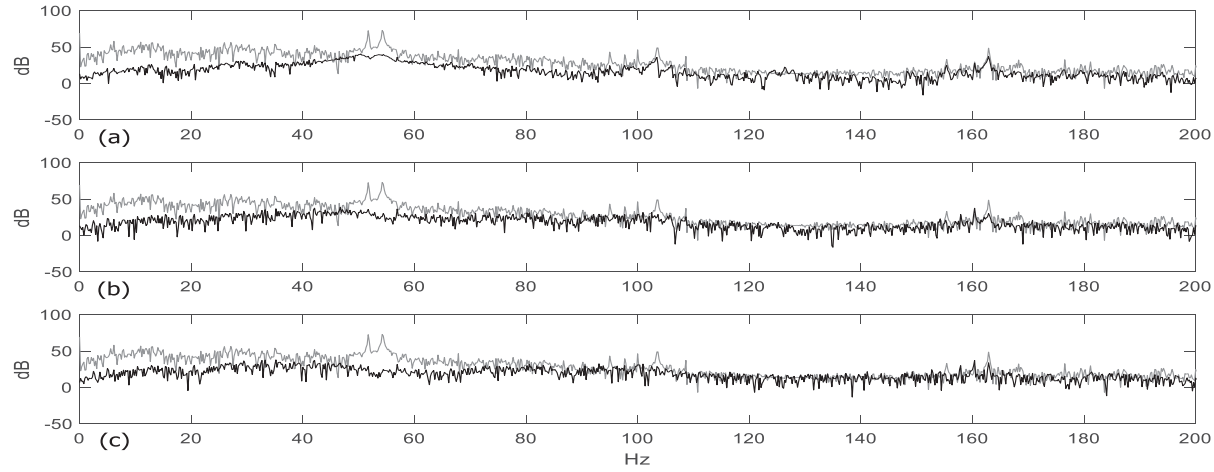

Figure 18: Spectrums of error (black) and desired (gray) signals for TFLN order size (a) 1, (b) 2 and (c) 3 (μ_t=0.001 and *BS*=30).

Freq. (Hz)	ANC OFF SPL (dB)	ANC ON/SPL (dB)		
		ORD=1	*ORD*=2	*ORD*=3
f_o=52	73.33	37.51	35.98	28.96
f_1=55	75.48	38.47	25.93	27.00

Table 5: TFLN controller performance in accordance to the order *ORD*.

Finally, the effect of the step size μ_t on the performance and the convergence behavior of the TFLN approach is studied for fixed values of order *ORD*=2 and buffer size *BS*=30.

Thus, as it is observed in Fig. 19, the MSEs computed over the last 15000 iterations are about -50, -48 and -40 dBs for μ_t 0.01, 0.001 and 0.0001, respectively. This means that the TFLN approach achieves an improved steady state MSE for μ_w close to 0.01. Also, the noise cancellation performance of TFLN controller with respect to step size μ_w is confirmed in the Table 6. As shown in Table 6, that the ANCS using μ_w =0.01 achieved up to 23 dB noise reduction at the desired 'beat' components f_o and f_1.

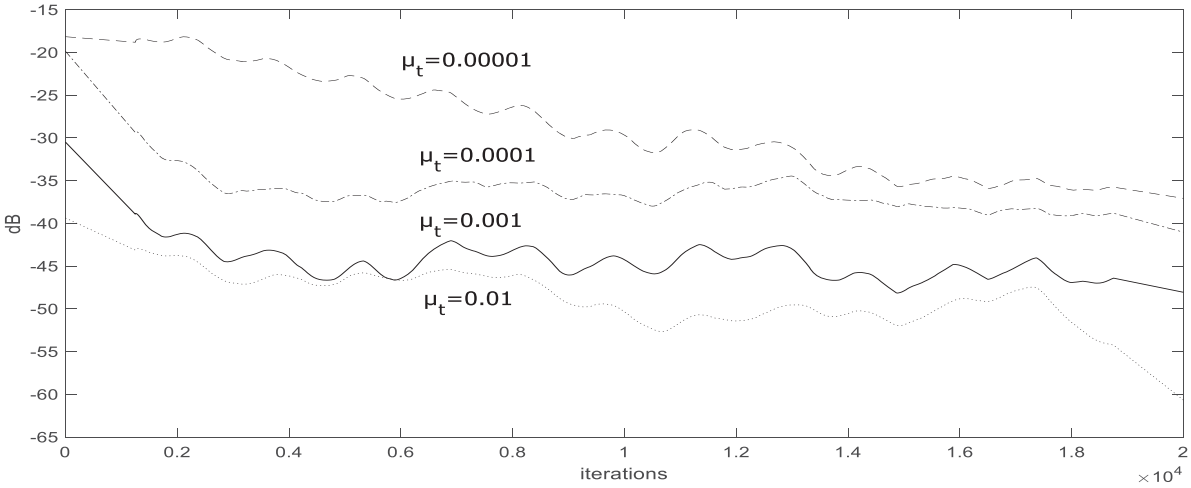

Figure 19: Comparison of convergence characteristics (MSE) obtained for different step sizes μ_t (*ORD*=2, and *BS*=30).

Freq. (Hz)	ANC OFF SPL (dB)	ANC ON/SPL (dB)		
		μ_t=0.0001	μ_t=0.001	μ_t=0.01
f_o=52	73.33	46.66	35.98	24.30
f_1=55	75.48	43.83	30.34	19.25

Table 6: TFLN controller performance in accordance to the step size μ_t.

5 CONCLUSIONS

In this paper the potential of applying a nonlinear active noise control system to reduce the levels of noise produced by two asynchronous diesel generators in the twin cabin of a luxury yacht has been investigated. It is difficult to control this using passive control treatments due to both weight and size limitations. Global active noise control is also not feasible due to the relatively wideband frequency content and the modally dense nature of the master cabin. Therefore, a practical active control system has been implemented which focuses a zone of

control at the head of the bed, where the generator noise is most disturbing when occupants are trying to sleep.

It has been shown that, due to the 'beat' components and their harmonics present in the disturbance noise spectrum, it is necessary to control multiple tones in order to achieve a significant level of narrowband attenuation. Therefore, a feedforward nonlinear control system has been investigated. It has been shown that this controller achieves significant narrowband attenuation in the sound pressure level at the error microphone located at the head of the bed. The performance, the stability as well as convergence of AEFLN and TFLN algorithms are dependent on the proper selection of the buffer size (*BS*) and the learning rates.

ACKNOWLEDGMENT

This research has been co-financed by the European Union and Greek national funds through the Operational Program Competitiveness, Entrepreneurship and Innovation, under the call RESEARCH – CREATE – INNOVATE (project code:T1EDK-3427)

REFERENCES

[1] S. Elliott, P. Nelson, I. Stothers, C. Boucher, In-flight experiments on the active control of propeller-induced cabin noise, *Journal of Sound and Vibration* 140(2), 219–38, 1990.

[2] LPR. de Oliveira, K. Janssens, P. Gajdatsy, H. Van der Auweraer, PS. Varoto, P. Sas, et al., Active sound quality control of engine induced cavity noise, *Mechanical Systems and Signal Processing* 23, 476–88, 2009.

[3] J. Cheer, SJ. Elliott, Multichannel control systems for the attenuation of interior road noise in vehicles, *Mechanical Systems and Signal Processing* 60–61, 753–769, 2015.

[4] K. Chen, R. Paurobally, J. Pan, X. Qiu, Improving active control of fan noise with automatic spectral reshaping for reference signal, *Applied Acoustics* 87, 142–152, 2015.

[5] S-P. Moon, JW. Lee, T-G. Chang, Performance analysis of an adaptive feedback active noise control based earmuffs system, *Applied Acoustics* 96, 53–60, 2015.

[6] T. Pamies, J. Romeu, M. Genesca, R. Arcos, Active control of aircraft fly-over sound transmission through an open window, *Applied Acoustics* 84, 116–121, 2014.

[7] P. Belanger, A. Berry, Y. Pasco, O. Robin, Y. St-Amant, S. Rajan, Multi-harmonic active structural acoustic control of a helicopter main transmission noise using the principal component analysis, *Applied Acoustics* 70(1), 153–164, 2009.

[8] J. Cheer, SJ. Elliott, Active noise control of a diesel generator in a luxury yacht, *Applied Acoustics* 105, 209–214, 2016.

[9] M. Wu, G. Chen, XJ. Qiu, An improved active noise control algorithm without secondary path identification based on the frequency domain subband architecture, *IEEE Transactions on Audio, Speech and Language Processing* 16(8), 1409–1419, 2008.

[10] S. Veena, SV. Narasimhan, Improved active noise control performance based on Laguerre lattice, *Signal Processing* 84(4), 695–707, 2004.

[11] SM. Kuo, DR. Morgan, Active noise control systems, algorithms and DSP implementations, *New York: Wiley*, 1996.

[12] OJ. Tobias, R. Seara, Performance comparison of the FXLMS, nonlinear FXLMS and leaky FXLMS algorithms in nonlinear active noise applications, Volume 1, 155–158: *Proceedings of the 11th European Signal Processing Conference*, 2004.

[13] NV. George, G. Panda, Advances in active noise control: a survey, with emphasis on recent nonlinear techniques, *Signal Processing* 93, 363–377, 2013.

[14] L. Lu, H. Zhao, Adaptive Volterra filter with continuous lp-norm using a logarithmic cost for nonlinear active noise control, *Journal of Sound and Vibration* 364, 14–29, 2016.

[15] Y. Pao, Adaptive Pattern Recognition and Neural Networks, Reading, *MA, USA: Addison-Wesley*, 1989.

[16] J. C. Patra, R. N. Pal, B. N. Chatterji, G. Panda, Identification of nonlinear dynamic systems using functional link artificial neural networks, *IEEE Transactions on Systems, Man, and Cybernetics, Part B* 29(2), 254–262, 1999.

[17] J C. Patra, Chebyshev neural network-based model for dual-junction solar cells, *IEEE Transactions on Energy Conversion* 26(1), 132–139, 2011.

[18] D. Comminiello, M. Scarpiniti, L. A. Azpicueta-Ruiz, J. Arenas-Garcia, A. Uncini, Functional link adaptive filters for nonlinear acoustic echo cancellation, *IEEE/ACM Transactions on Audio, Speech and Language Processing* 21(7), 1502–1512, 2013.

[19] JC. Patra, AC. Kot, Nonlinear dynamic system identification using Chebyshev functional link artificial neural networks, *IEEE Transactions on Systems, Man, and Cybernetics, Part B* 32(4), 505–511, 2002.

[20] JC. Patra, PK. Meher, G. Chakraborty, Nonlinear channel equalization for wireless communication systems using Legendre neural networks, *Signal Processing* 89(11), 2251–2262, 2009.

[21] P. Vinal, G. Vaibhav, H. Shashank, VG. Nithin, Design of Adaptive Exponential Functional Link Network-Based Nonlinear Filters, *IEEE Transactions on Circuits and Systems* 63(9), 2016.

[22] J. Jensen, S. Jensen, E. Hansen, Exponential sinusoidal modeling of transitional speech segments, Volume 1, 473–476: *Proceedings of IEEE International Conference of Acoustics, Speech and Signal Processing*, 1999.

[23] J. Jensen, J. H. Hansen, Speech enhancement using a constrained iterative sinusoidal model, *IEEE Transactions on Speech and Audio Processing* 9(7), 731–740, 2001.